J|A|C|S
ARTICLES
Published on Web 06/25/2002

Passive and Active Oxidation of Si(100) by Atomic Oxygen: A Theoretical Study of Possible Reaction Mechanisms

Cheol Ho Choi,[†] Da-Jiang Liu,[‡] J. W. Evans,[‡,§] and Mark S. Gordon*[,‡,⊥]

Contribution from the Department of Chemistry, College of Natural Sciences, Kyungpook National University, Taegu 702-701, South Korea, and Ames Laboratory, Department of Mathematics, and Department of Chemistry, Iowa State University, Ames, Iowa 50011

Received October 25, 2001

Abstract: Reaction mechanisms for oxidation of the Si(100) surface by atomic oxygen were studied with high-level quantum mechanical methods in combination with a hybrid QM/MM (Quantum mechanics/Molecular Mechanics) method. Consistent with previous experimental and theoretical results, three structures, "back-bond", "on-dimer", and "dimer-bridge", are found to be the most stable initial surface products for O adsorption (and in the formation of SiO_2 films, i.e., passive oxidation). All of these structures have significant diradical character. In particular, the "dimer-bridge" is a singlet diradical. Although the ground state of the separated reactants, O+Si(100), is a triplet, once the O atom makes a chemical bond with the surface, the singlet potential energy surface is the ground state. With mild activation energy, these three surface products can be interconverted, illustrating the possibility of the thermal redistribution among the initial surface products. Two channels for SiO desorption (leading to etching, i.e., active oxidation) have been found, both of which start from the back-bond structure. These are referred to as the silicon-first (SF) and oxygen-first (OF) mechanisms. Both mechanisms require an 89.8 kcal/mol desorption barrier, in good agreement with the experimental estimates of 80−90 kcal/mol. "Secondary etching" channels occurring after initial etching may account for other lower experimental desorption barriers. The calculated 52.2 kcal/mol desorption barrier for one such secondary etching channel suggests that the great variation in reported experimental barriers for active oxidation may be due to these different active oxidation channels.

1. Introduction

Due to their critical role in the processing of microelectronic devices, oxidation reactions on silicon surfaces have attracted considerable interest.[1] The outcome of exposing the Si(100) surface to atomic or molecular oxygen depends primarily on the surface temperature, T, and on the oxygen pressure, P.[2] In the low-T or high-P regime, one observes "passive oxidation", i.e., building up of an oxide film. In the high-T and low-P regime, one observes "active oxidation" or etching of the surface by removal of SiO. The two oxidation processes are

$$\text{passive oxidation:}\ \ Si(s) + O_2 \rightarrow SiO_2(s)$$

$$\text{active oxidation:}\ \ Si(s) + {}^1/{}_2O_2 \rightarrow SiO(g)$$

where s(g) denotes surface (gas phase) species. For typical pressures used in surface science studies, the transition from passive to active oxidation occurs at around 600−750 °C. Curves for oxygen uptake vs time display a transition from a simple Langmuir−Hinshelwood (LH) form for passive oxidation to a more slowly increasing but sigmoidal form (reflecting autocatalytic aspects of the oxide island formation process) upon entering the transition to active oxidation.

We will focus on the oxidation of Si(100), for which most previous studies have used molecular oxygen. However, for this (and other) system, there is considerable interest in comparison of atomic and molecular reactivity. Indeed, extensive studies also exist that have used atomic oxygen.[2,3] A central result that arises from comparing reaction with atomic and molecular oxygen is that the activation barrier for the key "slow" step in etching of SiO desorption is *identical* in both cases.[3] For molecular oxygen, there is a very low sticking probability (compared with unity for atomic oxygen), and likely an initial molecularly adsorbed state. However, it is believed[2−4] that this molecular adspecies quickly converts to (a pair of) the same adsorbed species as occurs in the deposition of atomic oxygen, and that this pair separates.[5] Hence, for the key slow step controlling the overall process, one is dealing with the same

* Corresponding author. E-mail: mark@si.fi.ameslab.gov.
† Kyungpook National University.
‡ Ames Laboratory, Iowa State University.
§ Department of Mathematicscs, Iowa State University.
⊥ Department of Chemistry, Iowa State University.

(1) *The Si−SiO$_2$ System, Material Science Monograph 32*; Balk, P., Ed.; Elsevier: Amsterdam, The Netherlands, 1988.
(2) (a) Engel, T. *Surf. Sci.* Rep. **1993**, *18*, 91. (b) Suemitsu, M.; Enta, Y.; Miyanishi, Y.; Miyamota, N. *Phys. Rev. Lett.* **1999**, *82*, 2334.
(3) For the review, see: (a) Engstrom, J. R.; Engel, T. *Phys. Rev. B* **1990**, *41*, 1038. (b) Engstrom, J. R.; Bonser, D. J.; Nelson, M. M.; Engel, T. *Surf. Sci.* **1991**, *256*, 317.
(4) Seiple, J. V.; Ebner, C.; Pelz, J. P. *Phys. Rev. B* **1996**, *53*, 15432.
(5) The diffusion barrier for O(s) is perhaps 2−3 eV, compared with a SiO desorption barrier of 4 eV. Thus, diffusion of adjacent O(s) pairs from molecular adsorption occurs before SiO desorption provided any extra barrier for the initial separation step is below ~1 eV

10.1021/ja012454h CCC: $22.00 © 2002 American Chemical Society

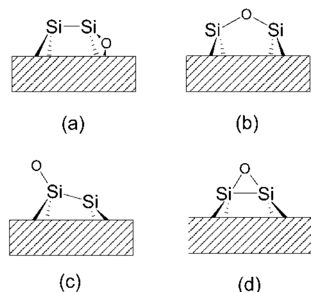

Figure 1. Previously suggested initial surface oxidation products: (a) back-bond, (b) dimer-bridge, (c) on-top, and (d) on-dimer structures.

situation as for atomic oxygen. Thus, we are motivated to explore in detail the simpler case of atomic oxygen, noting that results can for the most part be applied for molecular oxygen (after a suitable rescaling of the deposition flux).

Early studies focused on the determination of the formation of a stable oxide film on the silicon substrate,[6] identifying both the adsorbed species[7] and the structure of ultrathin oxide films.[8] In crystalline SiO_2, oxygen is in a bridging position between two silicon atoms; each silicon atom is in turn surrounded by four oxygen atoms in a tetrahedral configuration. This suggests that dicoordinated oxygen is the most abundant configuration in bulk silicon. HREELS (High-Resolution Electron Energy Loss Spectroscopy)[9] and SEXAFS (Surface Extended X-ray Adsorption Fine Structure)[10] measurements reveal Si−O−Si complexes, such as the "back-bond" and "dimer-bridge" arrangements shown in Figures 1, parts a and b, respectively. An "on-top" structure (Figure 1c) has also been proposed.[11a] Scanning tunneling microscopy (STM) has been used to study the oxidation process. However, the observed features such as position, height, and thermal stability are interpreted differently in different experiments. Avouris and Cahill[12] identified the observed bumps as isolated dimers comprised of Si atoms ejected from the surface, while Kliese et al.[13] concluded that they are weakly bound species of oxygen atoms or molecules.

With regard to computations, Smith and Wander[14] have investigated the adsorption of atomic oxygen on Si(100) using a $Si_{18}H_{24}O$ cluster model with Hartree−Fock wave functions and the STO-3G basis set[15] (HF/STO-3G), and predicted that atomic oxygen is adsorbed at the dimer bridge sites, Figure 1, **1b**. They further found that the dimer bridge (**1b**) and on-dimer (**1d**) sites become equivalent in the high coverage limit, giving rise to a 1 × 1 pattern. Using a slab model and local-density approximation, Miyamoto and Oshiyama have found three stable sites for the adsorption of atomic oxygen.[16] Of the three, the geometry in which the oxygen atom is inserted into the dimer bond ("dimer-bridge", **1b**) is predicted to be more stable than the on-dimer (**1d**) and back-bond (**1a**) sites. For dissociative adsorption of molecular oxygen, they found[17] that the back-bond site is the most stable. Using a first principles method based on the local density approach, Uchiyama and Tsukada[18] predicted that the back-bond site is more stable than the dimer-bridge site by 0.12 eV even in the case of atomic oxygen. Using calculations of STM images,[19] they showed that, in the filled states (negative applied surface bias voltage), the STM images for the back-bond and the dimer-bridge sites appear to be almost indistinguishable. The empty-states images (positive applied surface voltage) showed characteristic features of these two species.

There have been some attempts to understand the reaction mechanisms of the initial oxidation. Hoshino et al.[20] studied the symmetric mechanism of the direct insertion of molecular oxygen into the dimer bond using silicon cluster models containing two and nine silicon atoms, with the MP2/3-21G method. The activation energy required for this reaction was calculated to be 60.4 kcal/mol. These authors concluded that the reconstructed dimer is barely oxidized at room temperature and that defect sites may be the cause of the natural oxidation of Si-(100). This conclusion is consistent with some experiments[21] but contradicted others.[22] Since this symmetric path is formally symmetry forbidden, a lower energy asymmetric reaction pathway may exist. Conflicting theoretical results were obtained by Miyamoto and Oshiyama, who predicted using LDA slab models that the dissociative chemisorption of O_2 can occur without any activation barrier at all sites they studied.[16,17] Widjaja and Musgrave[23] recently studied the initial oxidation of the Si(100)-2×1 surface by O_2 with the B3LYP hybrid DFT method. Their calculated etching activation barriers are in the range of 65−67 kcal/mol. However, it will be shown in the current paper that the calculated numbers do not represent the correct etching barrier, since they considered the on-top structure as the starting configuration of the etching process.

Redondo and Goddard[24] were the first to illustrate that the bare surface dimer is highly diradical in nature. Therefore, methods based on single configurational wave functions, such as HF, MP2, and DFT, are not suitable for describing the multiconfigurational nature of the silicon surface. So the results from these types of calculations cannot be considered to be reliable.

Recently, using scanning reflection electron microscopy (SREM), Watanabe et al.[25] obtained strong evidence that the molecular O_2 oxidation of Si(100) proceeds in a layer-by-layer mode and that the first submonolayer including back-bonds is oxidized with almost no activation energy. Kato et al.[26] studied

(6) Deal, B. E.; Grove, A. S. *J. Appl. Phys.* **1965**, *36*, 3770.
(7) Morgen, P.; Hofer, U.; Wurth, W.; Umbach, E. *Phys. Rev. B* **1989**, *39*, 3720.
(8) Hollinger, G.; Himpsel, F. J. *Appl. Phys. Lett.* **1984**, *44*, 94.
(9) Schaefer, J. A.; Stucki, F.; Frankel, D. J.; Göpel, W.; Lapeyre, G. L. *J. Vac. Sci. Technol. B* **1984**, *2*, 359.
(10) Incoccia, L.; Balerna, A.; Cramm, S.; Kunz, C.; Senf, F.; Storjohann, I. *Surf. Sci.* **1987**, *189/190*, 453.
(11) (a) Engstrom, J. R.; Bonser, D. J.; Engel, T. *Surf. Sci.* **1992**, *268*, 238. (b) Westermann, J.; Nienhous, H.; Mönch, W. *Surf. Sci.* **1994**, *311*, 101. (c) Johnson, K. E.; Wu, P. K.; Sander, M.; Engel, T. *Surf. Sci.* **1993**, *290*, 213.
(12) (a) Avouris, P.; Cahill, D. G. *Ultramicroscopy* **1992**, *42−44*, 838. (b) Cahill, D. G.; Avouris, P. *Appl. Phys. Lett.* **1992**, *60*, 326.
(13) Kliese, P.; Röttger, B.; Badt, D.; Neddermeyer, H. *Ultramicroscopy* **1992**, *42−44*, 824.
(14) Smith, P. V.; Wander, A. *Surf. Sci.* **1989**, *219*, 77.
(15) (a) Hehre, W. J.; Stewart, R. F.; Pople, J. A. *J. Chem. Phys.* **1969**, *51*, 2657. (b) Collins, J. B.; Schleyer, P. v. R.; Binkley, J. S.; Pople, J. A. Self-Consistent Molecular Orbital Methods. 17. Geometries and binding energies of second-row molecules. A comparison of three basis sets. *J. Chem. Phys.* **1976**, *64*, 5142.
(16) Miyamoto, Y.; Oshiyama, A. *Phys. Rev. B* **1990**, *41*, 12680.
(17) Miyamoto, Y.; Oshiyama, A. *Phys. Rev. B* **1991**, *43*, 9287.
(18) Uchiyama, T.; Tsukada, M. *Phys. Rev. B* **1996**, *53*, 7917.
(19) Uchiyama, T.; Tsukada, M. *Phys. Rev. B* **1997**, *55*, 9356.
(20) Hoshino, T.; Tsuda, M.; Oikawa, S.; Ohdomari, I. *Phys. Rev. B* **1994**, *50*, 14999.
(21) Avouris, P.; Lyo, I.-W. *Appl. Surf. Sci.* **1992**, *60/61*, 426.
(22) (a) Engstrom, J. R.; Bonser, D. J.; Engel, T. *Surf. Sci.* **1992**, *268*, 238. (b) Westermann, J.; Nienhous, H.; Mönch, W. *Surf. Sci.* **1994**, *311*, 101. (c) Johnson, K. E.; Wu, P. K.; Sander, M.; Engel, T. *Surf. Sci.* **1993**, *290*, 213.
(23) Widjaja, Y.; Musgrave, C. B. *J. Chem. Phys.* **2002**, *116*, 5774.
(24) Redondo, A.; Goddard, W. A., III *J. Vac. Sci. Technol.* **1982**, *21*, 344.
(25) Watanabe, H.; Kato, K.; Uda, T.; Fujita, K.; Ichikawa, M.; Kawamura, T.; Terakura, K. *Phys. Rev. Lett.* **1998**, *80*, 345.

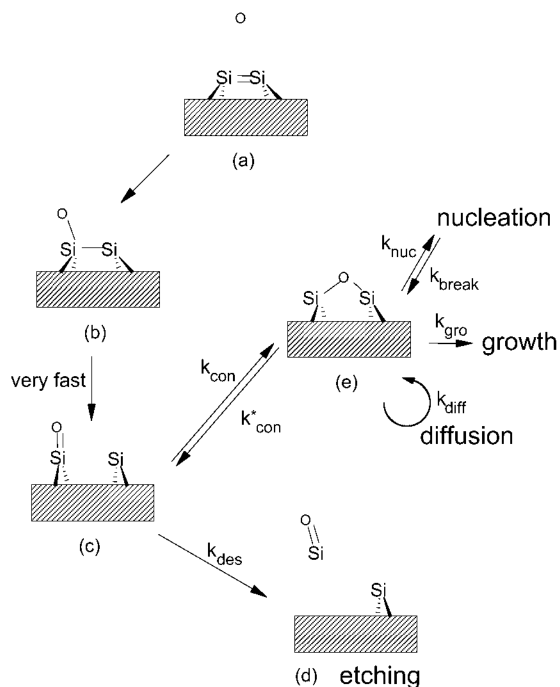

Figure 2. Previously suggested passive−active surface oxidation on the basis of experimental evidence. The initial oxidation product (b) is easily converted into a silanone, (c) which either makes an on-dimer structure (e) or etches the surface (d).

asymmetric pathways using spin-polarized DFT. The Si(100) surface was modeled as a repeated slab with a 4 × 2 unit cell, consisting of 10 layers of Si atoms and a vacuum spacing of the same thickness. They found that O_2 does not directly attack the back-bond. Rather, the oxidation occurs via metastable chemisorption states along barrierless reaction paths or channels.

The study of passive oxidation (building oxide film on a silicon surface) is of great technological relevance. In recent years, much effort has been devoted to the study of active oxidation and oxide decomposition to obtain a complete understanding of Si−SiO_2 interface formation using molecular and atomic oxygen.[3] Extensive earlier work comparing modulated molecular beam (MMB) and thermal desorption studies (TDS) at higher T by Engel and co-workers[2a] suggested the presence of two distinct adsorbed oxygen species, or at least distinct desorption behavior for isolated vs aggregated species. Seiple, Ebner, and Pelz[4] performed kinetic Monte Carlo (KMC) simulations using a single species model to reproduce morphological changes during the etching observed with STM. They favored a dual species model that reproduced the observed decoupling of the etching and nucleation rates. Suemitsu et al.[2b] performed rate equation analyses of oxygen uptake data from real-time UV photoelectron spectroscopy, again favoring a dual species model to capture some aspects of the T dependence of the initial uptake.

Figure 2 presents a schematic illustration of a dual-species oxidation model with atomic oxygen. This model assumes the existence of a "desorption precursor" configuration, **2c**, which may be described as a surface silanone species.[27] This silanone can either desorb from the surface as SiO (at rate k_{des}) or convert (at rate k_{con}) to a bridge or other more stable configuration **2e**. The latter can, in turn, diffuse across the surface (at rate k_{diff}) and lead to oxide-cluster nucleation (at rate k_{nuc}) or growth of oxide islands (at rate k_{gro}). Despite its importance, there has not been any ab initio theoretical attempt to elucidate these atomic mechanisms except the initial oxidations.

The most important parameter controlling the passive ⇔ active transition is the activation barrier, E_{des}, for removal of SiO from the surface. Previous estimates for E_{des} and the associated prefactor, ν, are $E_{des} = 79$ kcal/mol and $\nu = 10^{19}$/s from MMB experiments, and $E_{des} = 82-88$ kcal/mol and $\nu = 10^{16-18}$/s from TPD experiments.[2a,3] [The former is perhaps more relevant here given the low coverages of adsorbed oxygen, the latter applying to decomposition of SiO_2 films.]

There are a range of other estimates of E_{des} that are as low 40−50 kcal/mol.[28] The calculations presented in the following sections suggest that the low estimates for the activation energy may be due to "secondary etching mechanisms", in which SiO desorption occurs adjacent to vacancy defects created by previous etching.

To elucidate such complex surface phenomena, electronic structure descriptions of these reaction mechanisms and surface structures are crucial. In this paper, we attempt to unravel the detailed mechanisms of the initial stages of passive and active oxidation by atomic oxygen with the help of the newly developed SIMOMM (Surface Integration of Molecular Orbitals/Molecular Mechanics)[29] method, which facilitates the study of large surface cluster models. This method has proven to be useful in the study of silicon surface chemistry.[30]

2. Computational Details

Two basis sets were used in this work. The smaller basis set consists of the Hay−Wadt[31] effective core potential with d polarization functions, referred to as HW(d). To study basis set effects, we also used a combined basis set, referred to as "mixed", in which HW(d) is used for Si and 6-311G(d)[32] is used for O atoms. It is unlikely that diffuse functions are necessary, since no weakly bound (e.g., hydrogen bonded) or anionic species are present. The minimum energy reaction paths were determined by first optimizing the geometries of the minima and transition states. Then, each stationary point was characterized by computing and diagonalizing the Hessian matrix (matrix of energy second derivatives). To follow the minimum energy path (MEP), the Gonzalez−Schlegel second-order method[33] was used with a step size of 0.3 $amu^{1/2}$·bohr. Various points on the reaction paths, particularly transition states and intermediates, are often inherently multiconfigurational. Furthermore, near-degenerate or low-lying excited states with different spin states may exist. Therefore, methods based on a multiconfigurational wave function, including second-order energy corrections, are essential for consistent analyses of these reaction paths.

CASSCF (Complete active space SCF)[34] wave functions were used to optimize structures. The selected orbitals for the active space are

(26) Kato, K.; Uda, T.; Terakura, K. *Phys. Rev. Lett.* **1998**, *80*, 2000.
(27) Ludeke, R.; Koma, A. *Phys. Rev. Lett.* **1975**, *34*, 1170.
(28) (a) Hannon, J. B.; Bartelt, M. C.; Bartelt, N. C.; Kellog, G. L. *Phys. Rev. Lett.* **1998**, *81*, 4676. (b) Bartelt, M. C.; Hannon, J. B.; Schmid, A. K.; Stoldt, C. R.; Evans, J. W. *Colloids Surf. A* **2000**, *165*, 373. (c) Miyata, N.; Watanabe, H.; Ichikawa, M. *Phys. Rev. Lett.* **2000**, *84*, 1043. Note: Ref 28a assumes that the Arrhenius energy ($E = 2$ ev) for the etch rate equals the SiO desorption barrier, E_{des}. This applies for desorption-limited etching (but more generally one has $E < E_{des}$).
(29) Shoemaker, J. R.; Burgraff, L. W.; Gordon, M. S. *J. Phys. Chem. A* **1999**, *103* (17), 3245.
(30) (a) Choi, C. H.; Gordon, M. *J. Am. Chem. Soc.* **1999**, *121*, 11311. (b) Jung, Y.; Choi, C. H.; Gordon, M. S. *J. Phys. Chem. B* **2001**, *105* (18), 4039.
(31) Hay, P. J.; Wadt, W. R. *J. Chem. Phys.* **1985**, *82*, 270.
(32) (a) McLean, A. D.; Chandler, G. S. *J. Chem. Phys.* **1980**, *72*, 5639. (b) Krishnan, R.; Binkley, J. S.; Seeger, R.; Pople, J. A. *J. Chem. Phys.* **1980**, *72*, 650.
(33) (a) Gonzalez, C.; Schlegel, H. B. *J. Phys. Chem.* **1990**, *94*, 5523. (b) Gonzalez, C.; Schlegel, H. B. *J Chem Phys.* **1991**, *95*, 5853.

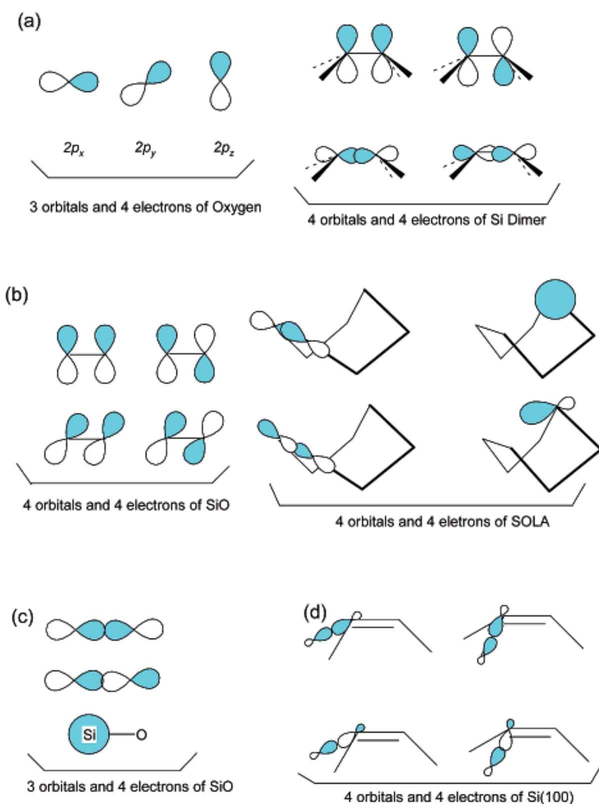

Figure 3. The active orbitals used in the calculations. (a) Three 2p oxygen orbitals and the bonding and the antibonding orbitals of Si dimer π, σ bonds. (b) Bonding and antibonding orbitals of the two π bonds, the bonding and antibonding orbitals of the newly formed Si−Si bond, and the two dangling bonds. (c) Bonding and antibonding orbitals of the Si−O σ bond, and the 3s orbital of the Si atom. (d) Two sets of bonding and antibonding orbitals of the Si−Si σ bonds. See text for detailed discussions.

now discussed in detail. As shown in Figure 3a, for the *passive* oxidation (O adsorption), a 7 orbitals and 8 electrons active space (8,7) is employed. This active space consists of the three 2p oxygen orbitals with the associated four electrons, plus the bonding and antibonding π and σ electrons and orbitals (i.e., (4,4)) in the Si−Si dimer bonds. Following common practice, the 2s oxygen orbital is excluded from the active space due to the large energy separation between 2s and 2p orbitals. This choice of active space therefore includes the "frontier" orbitals involved in reactions of atomic oxygen with a surface dimer. The nature of these active orbitals along the reaction path will be discussed below.

To choose the most appropriate set of active orbitals for the *active* oxidation (SiO desorption) process, the final reaction products (SiO + the Si surface with one less surface Si atom, referred to as SOLA) were considered. Preliminary calculations suggest that the SOLA forms one σ-type bond with some diradical character and two dangling bonds (Figure 3b). Therefore, the active space for active oxidation includes the π, π^* SiO orbitals and electrons (4,4), plus the bonding and antibonding orbitals of the newly formed Si−Si bond and the two dangling bonds (4,4), for a total of 8 orbitals and 8 electrons (8,8). Once the geometries of minima and transition states with these active spaces are determined, consistent energetics along the entire potential energy surface (O adsorption and SiO desorption alike) are obtained by using a (12,11) active space with 12 electrons in 11 orbitals. As shown in Figure 3c, the (12,11) active space is obtained by adding the σ,σ^* Si−O electrons and orbitals (2,2), and the Si 3s in Si−O (2,1) to the (8,8) space. As shown Figure 3d, the same (12,11) active space is obtained when one adds two sets of bonding and antibonding Si−Si σ,σ^* orbitals and electrons to the (8,7) passive oxidation active space of Figure 3a.

To recover the dynamic electron correlation, multireference second-order perturbation theory was used, since the level of accuracy for such methods is at least comparable to that of MP2 when single reference methods are appropriate.[35] The particular version of this method used in the present work is referred to as MRMP2 (multireference second-order perturbation theory).[36,37] Based on several calculations with the MRMP2 method[36,37] and the similar CASPT2 method,[38] the accuracy of relative energies predicted by MRMP2 with DZP is estimated to be in the range of ~5−10 kcal/mol. The GAMESS (General atomic and molecular electronic structure system)[39] program was used for all of the computations.

The differences among various QM/MM approaches arise in how the QM and MM portions of the model are linked. In IMOMM (Integrated Molecular Orbital/Molecular Mechanics),[40] the lengths of the connecting bonds remain fixed at user-selected values. However, for surface models, the high degree of connectivity in a lattice means there will be a large number of links between the QM and MM regions, resulting in the imposition of a large number of user-defined constraints. To avoid this, SIMOMM[41] removes the fixed geometric parameters during geometry optimization. MM3[42] parameters were used for the molecular mechanics optimization part of the computations.

As shown in Figure 4, the SIMOMM model used is composed of an $OSi_{15}H_{20}$ quantum region embedded in an $OSi_{136}H_{92}$ cluster. The quantum mechanical Si atoms are in purple and the O atom is in red. All of the computations were done without imposing symmetry unless otherwise specified.

3. Results and Discussion

A. O Adsorption Mechanisms. Before discussing the reaction mechanisms, it is important to note that the ground state oxygen atom is a triplet. Therefore, to properly understand the mechanisms, both singlet and triplet potential energy surfaces must be studied. Two possible reaction paths, the symmetric approach and the asymmetric approach, for the initial oxidation are shown in Figure 5a. First consider the *symmetric pathway*. The relevant structures are depicted in Figure 5, and the energetics are summarized in Figure 6 and Table 1. Preliminary studies,[43] including spin−orbit coupling effects,[44] suggest that along the symmetric approach, the triplet surface is repulsive and only the singlet surface has a minimum (depicted in Figure 5b) as the oxygen approaches the surface dimer. Therefore, assuming the reactants are initially in their ground electronic

(34) (a) Sunberg, K. R.; Ruedenberg, K. *In Quantum Science*; Calais, J. L., Goscinski, O., Linderberg, J., Ohrn, Y., Eds.; Plenum: New York, 1976. (b) Cheung, L. M.; Sunberg, K. R.; Ruedenberg, K. *Int. J. Quantum Chem.* **1979**, *16*, 1103. (c) Ruedenberg, K.; Schmidt, M.; Gilbert, M. M.; Elbert, S. T. *Chem. Phys.* **1982**, *71*, 41. (d) Roos, B. O.; Taylor, P.; Siegbahn, P. E. *Chem. Phys.* **1980**, *48*, 157. (e) Schmidt, M. W.; Gordon, M. S. *Annu. Rev. Phys. Chem.* **1998**, *49*, 233.

(35) (a) Werner, H.-J. *Mol. Phys.* **1996**, *89*, 645. (b) Schmidt, M. S.; Gordon, M. S. *Annu. Rev. Phys. Chem.* **1998**, *49*, 233. (c) Glaesemann, K. R.; Gordon, M. S.; Nakano, H. *PCCP* **1999**, 1, 967.

(36) (a) Nakano, H. *J. Chem. Phys.* **1993**, *99*, 7983. (b) Nakano, H. *Chem. Phys. Lett.* **1993**, *207*, 372.

(37) (a) Hirao, K. *Chem. Phys. Lett.* **1992**, *190*, 374. (b) Hirao, K. *Chem. Phys. Lett.* **1992**, *196*, 397. (c) Hirao, K. *Int. J. Quantum Chem.* **1992**, *S26*, 517. (d) Hirao, K. *Chem. Phys. Lett.* **1993**, *201*, 59.

(38) Roos, B. O.; Andersson, K.; Fulscher, M. K.; Malmqvist, P.-A.; Serrano-Andres, L.; Pierloot, K.; Merchan, M. *Adv. Chem. Phys.* **1996**, *93*, 219.

(39) (a) Schmidt, M. W.; Baldridge, K. K.; Boatz, J. A.; Elbert, S. T.; Gordon, M. S.; Jensen, J. H.; Koseki, S.; Matsunaga, N.; Nguyen, K. A.; Su, S.; Windus, T. L.; Dupuis, M.; Montgomery, J. A., Jr. *J. Comput. Chem.* **1993**, *14*, 1347. (b) Fletcher, G. D.; Schmidt, M. W.; Gordon, M. S. *Adv. Chem. Phys.* **1999**, *110*, 267.

(40) Maseras, F.; Morokuma, K. *J. Comput. Chem.* **1995**, *16*, 1170.

(41) (a) Shoemaker, J. R.; Burggraf, L. W.; Gordon, M. S. *J. Phys. Chem. A* **1999**, *103*, 3245. (b) Shoemaker, J. R.; Burggraf, L. W.; Gordon, M. S. *J. Chem. Phys.* **2000**, *112*, 2994.

(42) (a) Allinger, N. L.; Yuh; Y. H.; Lii, J. H. *J. Am. Chem. Soc.* **1989**, *111*, 8551. (b) Lii, J. H.; Allinger, N. L. *J. Am. Chem. Soc.* **1989**, *111*, 8566. (c) Lii, J. H.; Allinger, N. L. *J. Am. Chem. Soc.* **1989**, *111*, 8576.

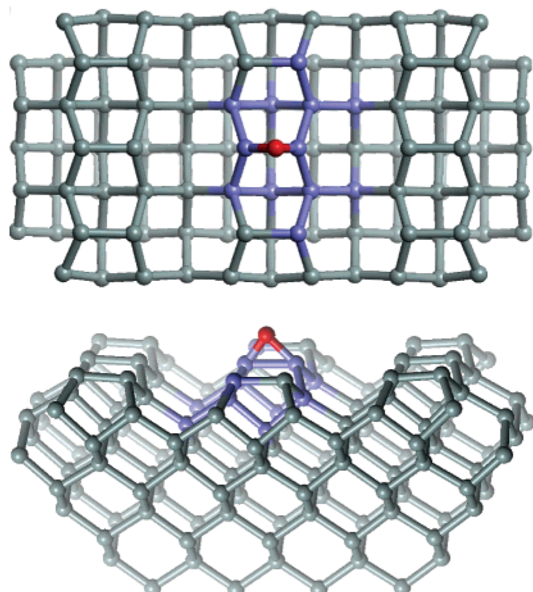

Figure 4. The SIMOMM model of the $OSi_{15}H_{20}$ quantum region embedded in an $OSi_{136}H_{92}$ MM cluster, where the MM atoms are calculated with MM3 parameters.

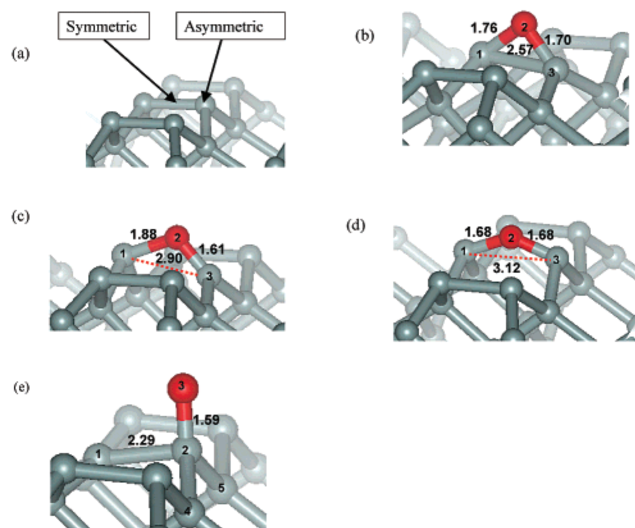

Figure 5. The minima and transition state along the symmetric approach of initial oxidation as obtained with SIMOMM:CASSCF(8,7)/HW(d): (a) two possible approaches; (b) on-dimer structure; (c) transition state that connects b and d; (d) dimer-bridge structure; and (e) transition state connecting **8a** and **5b**.

states, intersystem crossing from the triplet to the singlet surface must occur at some point along the initial symmetric approach of O to the surface, to obtain **5b**. A nonadiabatic treatment including spin−orbit coupling could, of course, give rise to a barrier at such a crossing. A more detailed analysis of this phenomenon will be published elsewhere.[44] Aside from the intersystem crossing, **5b** is formed with no intervening barrier, indicating that the atomic oxygen adsorption process follows a similar path to that of O_2 adsorption as suggested by earlier theoretical studies.[16,17,26] These results are in contrast to previous MP2/3-21G calculations[20] that predicted a large activation

(43) The preliminary calculations adopted a model constructed with 9 Si atoms and 1 O atom. A CASSCF(8,7) active space, composed of three O p orbitals and Si dimer π and σ bonding−antibonding pairs, was employed.

(44) Choi, C. H.; Gordon, M. S. In preparation.

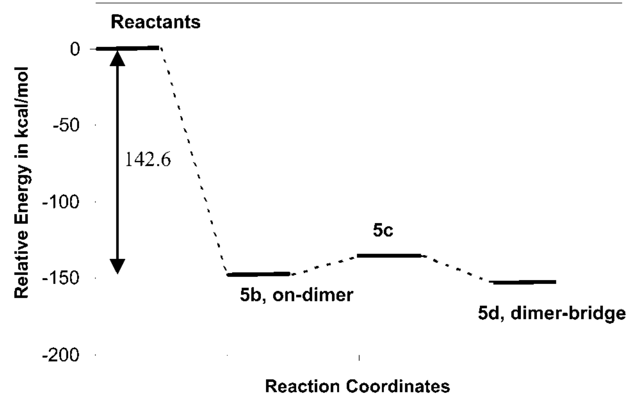

Figure 6. Relative energy diagram of structures in Figure 5 along the symmetric approach. Energies are obtained with SIMOMM:MRMP2-(12,11)/MIXED at SIMOMM:CASSCF(8,7)/HW(d) geometries.

barrier. The singlet is the ground state for the remainder of the symmetric part of the potential energy surface (PES). Since the remainder of the ground-state potential energy surface is a singlet, all energies discussed below are presented relative to the singlet reactants including the excited O (^{1}D) state.

Structure **5b** corresponds to the "on-dimer" structure, **1d**. The SIMOMM:CASSCF(8,7)/HW(d) Si−O bond lengths are calculated to be 1.70 and 1.76 Å, illustrating an asymmetric structure that has not been proposed previously. The Si_1-Si_3 bond length is calculated to be 2.57 Å, somewhat longer than a typical Si−Si single bond distance of 2.34 Å. This on-dimer structure **5b**, which still has a Si_1-Si_3 bond, is lower in energy than the singlet reactants (free oxygen + bare surface) by 142.6 kcal/mol at the SIMOMM:MRMP2/mixed level of theory. The effect of using this mixed basis set compared with HW(d) is small (see Table 1), while increasing the active space from (8,7) to (12,11) increases the relative stabilization energy of **5b** by about 20 kcal/mol indicating some multiconfigurational character. The dimer bridge structure **5d** is more stable than the singlet reactants by 150.0 kcal/mol. [Note that the triplet reactant is 16.3 kcal/mol more stable than the singlet reactant (see Table 1)]. It is formed by traversing the transition state **5c**, in which the Si−Si σ bond is being broken. In structure **5d**, the two Si−O bond lengths are 1.67 Å, somewhat smaller than those of **5b**, indicating the formation of strong Si−O bonds. The Si_1-Si_3 distance is 3.12 Å, suggesting that the Si−Si bond has been broken. The barrier for the reaction **5b** → **5d** is 11.3 kcal/mol, and **5d** is 7.4 kcal/mol lower in energy than **5b** on the singlet surface (see Figure 6 and Table 1).

Figure 7, **7a** and **7b**, presents schematics and associated natural orbital occupation numbers (NOON) for the Si_1-Si_3 bonding and antibonding orbitals in structures **5b** and **5d**, respectively. The NOON of **7a** show significant deviation from a closed shell structure, indicating strong diradical character in the Si_1-Si_3 bond. Once this bond is broken as shown in **7b**, the system becomes a singlet diradical. This illustrates the requirement that analysis of this potential energy surface requires a multiconfigurational description. These computational results show that the on-dimer and dimer-bridge structures may coexist on the surface, at least initially, and that they can be easily interconverted with mild thermal activation.

The structures and energetics along the *asymmetric pathway* are presented in Figures 8 and 9 and Table 2. In contrast to the symmetric pathway where only the singlet surface is attractive,

Table 1. Relative Energies of Minima and Transition State Along the Symmetric Passive Oxidation Approach (kcal/mol)

		reactants	**5b**, on-dimer	**5c**, TS	**5d**, dimer-bridge
singlet state	CASSCF(7,8)/HW(d)	0	−111.0	−117.1	−126.0
	CASSCF(12,11)/HW(d)	0	−131.7	−119.7	−162.2
	MRMP2[a](12,11)/HW(d)	0	−147.4	−135.3	−152.3
	MRMP2(12,11)/MIXED	0	−142.6	−131.3	−150.0
triplet state	CASSCF(11,12)/HW(d)	−10.1			
	MRMP2(11,12)/HW(d)	−16.3			

[a] The particular MRMP2 used in this study is MCQDPT2 (multi-configurational quasi-degenerate second-order perturbation theory). [b] All calculations are done with the SIMOMM($OSi_{15}H_{20}$; $OSi_{136}H_{92}$) model as shown in Figure 4. [c] All geometries are obtained with SIMOMM:CASSCF(8,7)/HW(d). [d] All energies are QM + MM energies. [e] All energies are relative to the singlet state reactants (separated bare silicon surface + O atom).

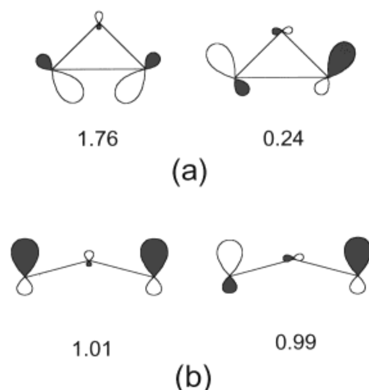

Figure 7. Illustrations of two orbitals in the (12,11) active space along with the corresponding NOON: (a) corresponds to **5b** and (b) corresponds to **5d**.

the singlet and triplet surfaces of the asymmetric pathway are both attractive initially. However, Figure 9 presents only the singlet surface, since energetically the singlet surface beyond the first step is lower than the triplet (see Table 2 for the detailed energies of both the singlet and triplet). All singlet and triplet structures have been optimized at the CASSCF(8,7)/HW(d) level of theory.

The entire singlet potential energy surface (for both O adsorption and SiO desorption) is presented in Figure 9. The initial surface product of the asymmetric approach is **8a**, which may be described as an "on-top" structure, as illustrated in Figure 1, **1c**. The Si_2-O_3 bond lengths are 1.56 and 1.71 Å for the singlet and triplet structures, respectively. The corresponding Si_1-Si_2 bond lengths are 2.54 and 2.37 Å. **8a** is 111.2 kcal/mol more stable than the reactants. The MRMP2(12,11)/HW(d) singlet **8a** is 7.2 kcal/mol more stable than the corresponding triplet. Transition state **8b** connects **8a** and **8c**. The latter may be described as a "back-bond" structure (cf., Figure 1, **1a**), in which the oxygen atom is inserted into a bond connecting a surface Si and a Si in the next layer by breaking the Si_2-Si_4 bond. The Si_4-O_3 distance in the singlet transition state, **8b**, is about 0.4 Å longer than that in the corresponding triplet state. The singlet activation barrier is 4.2 kcal/mol and **8c** is 34.9 kcal/mol more stable than **8a**. This suggests that with mild thermal activation, **8a** is easily converted into **8c**. So, the back-bond structure **8c** is the most stable product arising from the asymmetric O adsorption, only a few kilocalories per mole higher in energy than the global minimum dimer bridge, **5d**. These relative energies are consistent with the results of the DFT LDA slab model calculations,[16] but not with another LDA calculation[18] that predicts the back-bond structure to be the global minimum. The more sophisticated calculations presented here are likely to be more reliable.

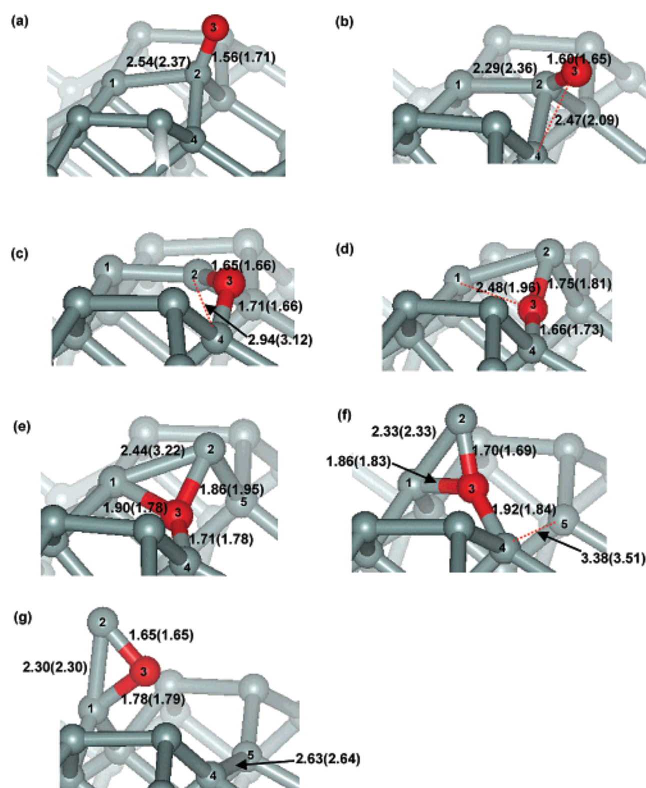

Figure 8. The minima and transition state along the asymmetric passive oxidation (O adsorption) approach and the SF (Silicon First) leaving mechanism for etching as obtained with SIMOMM:CASSCF(8,7)/HW(d): (a) on-top structure; (b) transition state connecting a and c; (c) back-bond structure;. (d) transition state connecting c and e; (e) minimum with trivalent oxygen atom; (f) transition state connecting e and g; and (g) minimum with triangle configuration. Numbers in parentheses are triplet geometries.

The Si−O bond lengths in **8c**, back-bond, are 1.65 and 1.71 Å. These are similar to those of the dimer bridge structure, **5d**. The fact that **8c**, **5b**, and **5d** are similar in energy, in addition to the small energy barriers leading to these structures, suggests that these structures may be the most important structures in the initial stage of surface oxidation.

The natural orbital occupation numbers for the active orbitals in structure **8a** are 1.99, 1.98, 1.97, 1.97, 1.97, 1.94, 0.06, 0.03, 0.03, 0.03, and 0.02, and those of **8c** are 1.99, 1.98, 1.98, 1.98, 1.97, 1.88, 0.12, 0.03, 0.02, 0.02, and 0.02. This suggests that **8a** is essentially closed shell, whereas **8c** has significant multiconfigurational character (the 1.88 and 0.12 NOON in **8c** correspond to the π and π^* Si_1-Si_2 orbitals).

In summary, the initial O adsorption processes result in three stable structures **8c**, **5b**, and **5d**, before further diffusion of O atoms into the silicon bulk. Of these, **8c** shall be shown to be

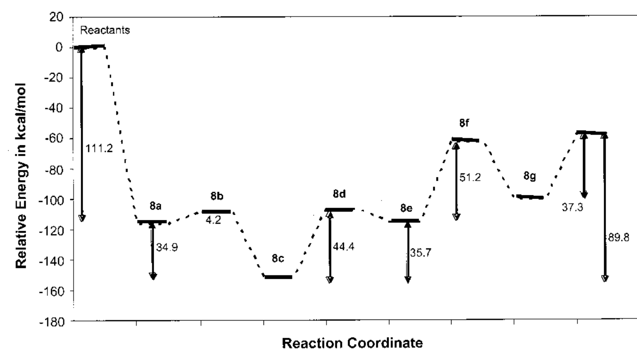

Figure 9. Relative energy diagram along the asymmetric approach and the SF (Silicon First) leaving mechanism for active oxidation (etching). Energies are obtained with SIMOMM:MRMP2(12,11)/MIXED at SIMOMM:CASSCF(8,7)/HW(d) geometries.

Table 2. Relative Energies of Minima and Transition State Along the Asymmetric Passive Oxidation Approach in kcal/mol

		8a, on-top	8b, TS	8c, back-bond
singlet potential	CASSCF(12,11)/HW(d)	−96.8	−89.1	−145.8
	MRMP2(12,11)/HW(d)	−108.2	−110.7	−150.6
	MRMP2(12,11)/MIXED	−111.2	−107.0	−146.1
triplet potential	CASSCF(12,11)/HW(d)	−94.4	−89.0	−137.4
	MRMP2(12,11)/HW(d)	−98.6	−104.0	−132.2

[a] All calculations are done with the SIMOMM($OSi_{15}H_{20}$; $OSi_{136}H_{92}$) model as shown in Figure 4. [b] All geometries are obtained with SIMOMM: CASSCF(8,7)/HW(d). [c] All energies are QM + MM energies. [d] All energies are relative to the singlet state reactant (separated bare silicon surface and O atom).

the starting point of the SiO desorption process in Section D below. Thus, the remainder of Figure 8 pertains to the desorption process.

B. Surface Conversion between "On-Dimer" and "On-Top" Structures. In the foregoing, we allude to conversion between the three similar low-energy structures **8c** (back-bond), **5b** (on-dimer), and **5d** (dimer bridge). Recall that the barrier for conversion between the dimer bridge and on-dimer species (via transition state **5c**) is identified in Figure 6. It is interesting to consider if the back-bond structure can convert directly to one of these two species (most likely the dimer bridge). In fact, our analysis finds no such direct pathway. However, indirect conversion is possible through the transition state **5e** that connects the on-dimer and the on-top structures (recalling that the back-bond species can be reached from the on-top structure; see Figure 9). The relative MRMP2(12,11)/MIXED energies along the reaction path for this conversion are presented in Figure 10. At this level of theory, the reaction barrier from **5b** to **8a** is calculated to be 65.2 kcal/mol, while the reverse barrier is 34.3 kcal/mol. At surface temperatures near 1000 °C, this reaction can easily be achieved, resulting in a redistribution of the initial surface products. Recall that the back-bond species can be reached from the on-top species (see Figure 9), and that the dimer bridge species can be accessed from the on-dimer species (Figure 6)

C. Local Surface Relaxation of the Etched Surface. Before discussing the active oxidation mechanisms, it is informative to discuss the etched surface, SOLA, after one Si atom has been removed by an O atom. This preliminary analysis was performed with CASSCF(4,4)/HW(d) wave functions. As shown in Figure 11a, before the active oxidation, the Si_1-Si_3 distance is calculated to be 3.99 and 3.86 Å for the singlet and triplet states,

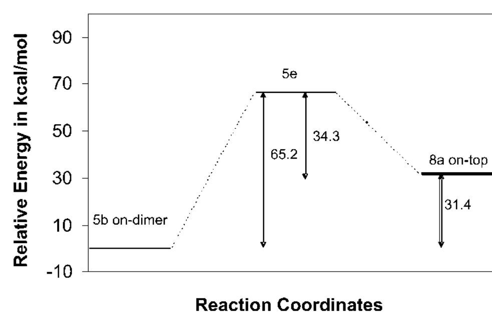

Figure 10. Relative energy diagram along the surface conversion reaction path. Energies are obtained with SIMOMM:MRMP2(12,11)/MIXED at SIMOMM:CASSCF(8,7)/HW(d) geometries.

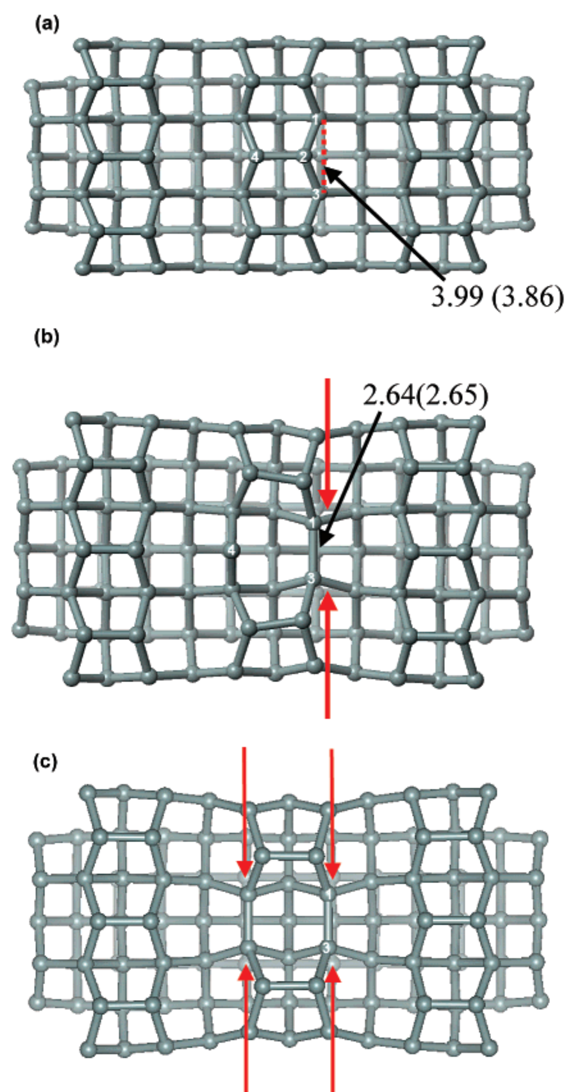

Figure 11. Illustration of the relaxation of the SOLA: (a) before etching and (b) after etching. Geometries are obtained with SIMOMM:CASSCF-(4,4)/HW(d). Numbers in parentheses are triplet geometries.

respectively. When atom Si_2 in the surface dimer (Figure 11a) is removed by active oxidation, resulting in Figure 11b, a new Si_1-Si_3 bond is formed, leaving Si_4 as a diradicaloid silylene. The length of the new Si_1-Si_3 bond is calculated to be 2.64 Å (2.65 Å for the triplet), somewhat longer than a typical Si−Si single bond length of 2.34 Å. The nearby surface structure relaxes laterally relative to the top-most layer of Si dimers. As a result, the geometries of the nearby Si dimers are distorted.

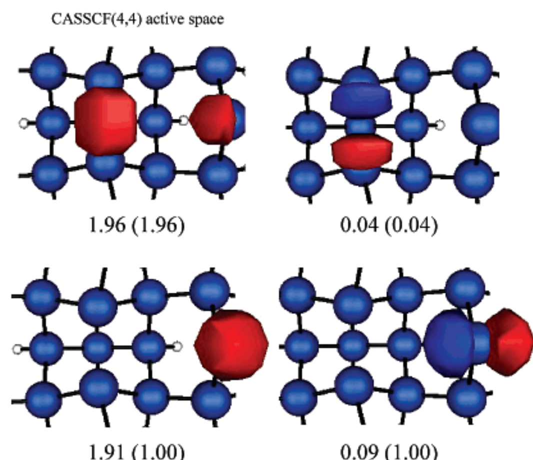

Figure 12. The SIMOMM:CASSCF(4,4)/HW(d) orbitals and NOON (Natural Orbital Occupation Number) of the SOLA active space. Numbers in parentheses are triplet NOON. The active orbitals are the two dangling bonds of Si_4 and the bonding and antibonding orbitals of Si_1-Si_3. Since these are the natural orbital representations, the two dangling bonds are presented as localized s and p_z orbitals that are almost parallel to the surface. It would be also possible to obtain two identical dangling bonds with appropriate linear combinations of the two orbitals. The red/blue colors represent different phases ($\pm$) of the wave function.

This effect is passed along to nearby Si dimers. So this local surface is subjected to geometric strain. The singlet state for this reconstructed etched surface is more stable than the triplet by 7.2 kcal/mol. It can easily be imagined that such relaxations further activate the nearby surface atoms, facilitating subsequent oxidations/etching. In addition, the active oxidation process leaves reactive diradicaloid silicon atoms behind (e.g., Si_4). Therefore, one can speculate that, once the initial active oxidation occurs, subsequent oxidations/etching require much less activation energy due to this "auto-catalytic" preparation of the surface in the first step. This is discussed further in Section E.

The active orbitals used in these calculations on **11b**, along with the natural orbital occupation numbers (NOON), are shown in Figure 12. Note that the single configuration Hartree−Fock method incorrectly predicts the triplet state to be the ground state of **11b**. The diradical nature of the bare surface dimer **11a** has been discussed in previous papers.[24,28,29,45] The active orbitals for structure **11b** are the two dangling bonds (equivalently Si lone pair and empty p orbital) of Si_4 and the bonding and antibonding orbitals of Si_1-Si_3. The NOON indicate that Si_4 has nonnegligible occupation of the empty p orbital in the singlet state.

D. SiO Desorption Mechanisms (Etching/Active Oxidation). To study this part of the potential energy surface, the 8 orbitals and 8 electrons (8,8) active space discussed earlier was used to optimize the minima and transition state structures. Then, the (12,11) active space was used to obtain energies. Two active oxidation channels, referred to as the Si-first (SF) and O-first (OF) SiO-desorption mechanisms, have been found. Note that both mechanisms require the "back-bond" structure (**1a**, **8c**) as a starting point.

According to our CASSCF(8,8) results, both mechanisms are predicted to have no net reaction barrier other than the enthalpy changes. In other words, the energy difference between the back-bond and the reaction products (SiO molecule + surface) is the same. The difference between the two channels is that depending on the details of the mechanism, the heights of "internal" barriers (barriers whose energies are less than that of the reactants) differ. (See Table 3.)

First consider the SF mechanism in detail. **8d**−**8g** in Figure 8 represent the minima and transition states along the SF mechanism. A schematic of the reaction path connecting these stationary points is presented in Figure 9. Transition state **8d** connects the minima **8c** and **8e**. In **8d**, the oxygen tries to make another O−Si bond with the Si_1 atom of the surface dimer. The activation barrier at **8d** is 44.4 kcal/mol. The singlet and triplet states of **8d** have quite different geometries, particularly the Si_1-O_3 distance. The intermediate **8e** has an unusual structure, in which oxygen is trivalent, bonded to three Si atoms. The transition state **8f** connects **8e** and **8g**. In the latter structure, a new Si_4-Si_5 bond has been formed and the O_3-Si_4 bond has been broken. An $Si_1-O_3-Si_2$ three-membered ring is attached to the Si surface by two Si−Si bonds at Si_1. The reaction barrier at transition state **8f** (see Figure 9) is 51.2 kcal/mol. In **8f**, the Si_2-Si_5 bond is broken making a radical at Si_5. In **8g**, the radical at Si_5 makes a bond with Si_4 (2.63 Å). With a final 37.3 kcal/mol of activation energy, the Si_2-O_3 molecule desorbs from the surface (see Figure 9) yielding the newly formed Si_4-Si_5 bond and a silylene at Si_1, **11b**.

The overall activation barrier between the back-bond structure **8c** and final products is 89.8 kcal/mol. This is in good agreement with experimental estimates of 80−90 kcal/mol, strongly suggesting that the back-bond structure is the likely starting point for the SiO desorption. The dimer-bridge, **5d**, and on-dimer, **5b**, structures also may be actively oxidized. However, no direct active oxidation channels that start from these surface species have been found. The calculations therefore suggest that these two species must first be converted into **8c** to be actively oxidized. Of course, each step in these conversion processes requires an additional activation energy. For instance, to convert the on-dimer structure **5b** to **8c** via the intermediate **8a** requires a net 65.2 kcal/mol activation energy (see Figure 10). Likewise, the activation energy to convert the dimer-bridge **5d** to **8c** via intermediate **5b** is 18.7 kcal/mol. So, according to the SF mechanism, the initial active oxidation occurs at the back-bond site. For the on-dimer or dimer-bridge sites to be actively oxidized, they must first be converted into the back-bond structure.

Now consider the OF SiO-desorption mechanism that also starts from the back-bond site. As discussed above, in the OF mechanism, the reaction barrier of the initial TS is nearly as large as the energy difference between the back-bond structure and products. The structures are presented in Figure 13. Transition state **13a** connects back-bond **8c** and intermediate **13b**. In **13a**, Si_2-Si_5 is elongated to 2.70 Å, and O_3-Si_4 is broken. This TS is very unstable, since it is breaking two Si−Si bonds. This results in a CASSCF(8,8)/HW(d) activation barrier of 101.1 kcal/mol. This represents nearly all of the stabilization energy of the back-bond structure (101.9 kcal/mol at the same level of theory). The minimum **13b** is only 19.4 kcal/mol lower in energy than **13a**. In **13b**, a new Si_4-Si_5 bond is formed as in **8g**. TS **13c** connects **13b** with **13d**. The reaction barrier at **13c** is 19.2 kcal/mol; the Si_1-Si_2 bond is elongated to 3.26 Å in this TS. Structure **13d** is a van der Waals complex, with only a tiny stabilization energy of 0.1 kcal/mol relative to

(45) Radeke, M. R.; Carter, E. A. *Phys. Rev. B* **1996**, *54*, 11803.
(46) Venables, J. A. *Philos. Mag.* **1973**, *27*, 693.

Table 3. Relative Energies of Minima and Transition States Along the Etching Path (kcal/mol)

		8d, TS	8e	8f, TS	8g	products
singlet potential	CASSCF(12,11)/HW(d)	−105.8	−111.2	−79.1	−94.1	−52.7
	MRMP2(12,11)/HW(d)	−106.0	−115.0	−62.0	−99.9	−56.9
	MRMP2(12,11)/MIXED	−101.7	−110.4	−59.2	−93.6	−56.3
triplet potential	CASSCF(12,11)/HW(d)	−82.8	−93.6	−50.0	−74.0	−46.8
	MRMP2(12,11)/HW(d)	−88.7	−92.9	−49.7	−69.7	−50.6

[a] All calculations are done with the SIMOMM($OSi_{15}H_{20}$; $OSi_{136}H_{92}$) model as shown in Figure 4. [b] All geometries are obtained with SIMOMM:CASSCF(8,7)/HW(d). [c] All energies are QM + MM energies. [d] All energies are relative to the singlet state reactant (separated bare silicon surface and O atom).

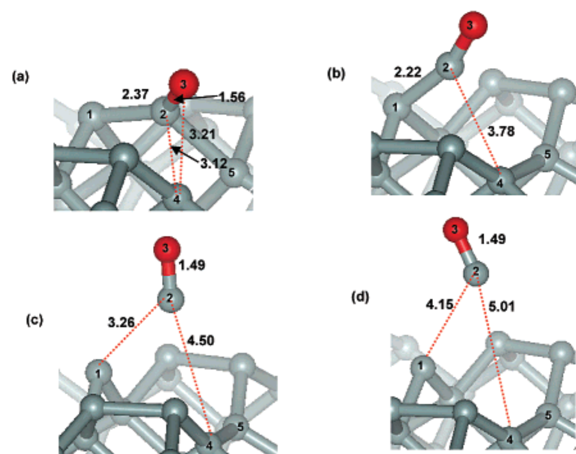

Figure 13. The minima and transition state along the OF (Oxygen First) leaving mechanism for etching obtained with SIMOMM:CASSCF(8,7)/HW(d): (a) transition state connecting **8c** and **13b**; (b) minimum; (c) transition state connecting b and d; and (d) van der Waals complex.

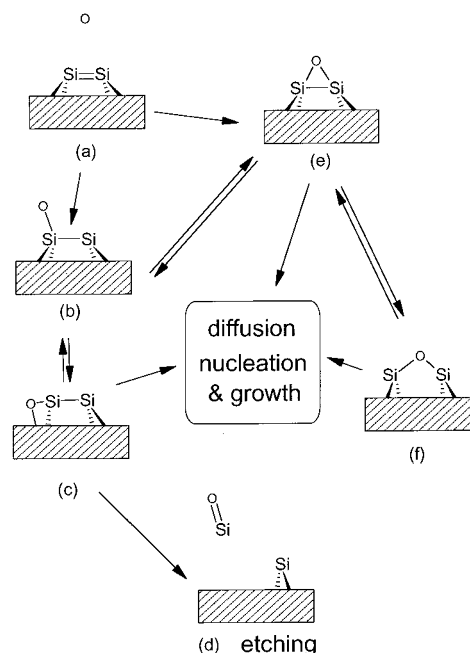

Figure 14. Proposed mechanism for the passive−active surface oxidation. Two approaches (symmetric and asymmetric) initially yield on-top (b) and on-dimer (e) structures. The on-top structure is converted into either back-bond (c) or on-dimer (e). The back-bond structure is necessary to etch the surface. The dimer-bridge structure does not participate in etching.

13c, and just 0.1 kcal/mol relative to the final active oxidation product. Therefore, **13c** and **13d** are very small ripples on the PES that may not actually exist at higher levels of theory.

E. Overview of the Primary Oxidation Process. On the basis of these results, we propose a new scheme for surface oxidation as presented in Figure 14. The on-top, **14b**, and on-dimer, **14e**, structures may be formed initially. There will be surface interconversion between these two species, leading to the possibility of redistribution of the surface products. The on-top structure is easily converted into the back-bond species, **14c**, that is ultimately responsible for the surface etching, **14d**. The on-dimer species is also easily converted into a dimer-bridge, **14f**, that is responsible for other surface reactions, such as diffusion, growth, and nucleation. Of course, the back-bond is also responsible for the surface oxide film growth in the low surface temperature regime. According to this picture, the surface silanone structure, **2c**, does not appear to exist, at least not when there is a nearby reactive silylene adjacent to the silanone.

The picture presented in Figure 14 (together with our results for energetics) is fundamentally different from the commonly held view indicated in Figure 2 (together with additional assumptions leading to the so-called dual-species model). This common view is that in addition to the lower energy species (Figure 2e), there exists a second more weakly bound silanone species (Figure 2c), which plays a key role in etching since $k_{des} \gg k_{con}$ (i.e., desorption occurs more readily than conversion). In our analysis, the only candidate for the second species is the on-top structure, but the barrier for conversion to the rather more stable back-bond structure (and the barriers for conversion of this structure to on-dimer and dimer bridge structures) is much lower than the barrier for SiO desorption. Thus, the conditions for the dual species model are not satisfied: there is no weakly bound species (relative to the back-bond, on-dimer, and dimer-bridge species) that can desorb more readily than convert.

It should be noted that the dual species model has been viewed as necessary to explain discrepancies between MMB and TPD estimates of SiO desorption barriers,[2a] and to explain the decoupling of etching rates and nucleation rates of oxide nucleation.[4] However, the difference between MMB and TPD results may also be explained by cooperativity in the desorption process.[2a] In the dual-species picture, reduction of the nucleation rates while the etch rate remained constant was associated with independent densities of silanone (controlling etching) and the lower energy species (controlling oxide nucleation). However, application of standard nucleation theory[46] shows that the nucleation rate should decrease much more quickly with time than the etch rate, especially for reversible formation of oxide islands. This applies under quite general conditions of diffusion-mediated growth of oxide islands. In addition, the reduction of nucleation (with approximately constant etch rate) could also result from kinetic roughening as etching proceeds.

F. Secondary Etching Mechanisms. It is expected that since such a silylene center is unstable, it can be easily oxidized. Once etching has begun, a supersaturation of various vacancies develops on the Si(100) surface. Such vacancies adjacent to

Table 4. Relative Energies of Minima and Transition State Along the Secondary Etching Path (SEOF) (kcal/mol)

	16a	**16b**, TS	**16c** + SiO
CASSCF(12,11)/HW(d)	−136.8	−72.5	−117.9
MRMP2(12,11)/HW(d)	−139.4	−76.2	−119.1
MRMP2(12,11)/MIXED	−136.2	−74.0	−118.1

[a] All calculations are done with the initial reactant, SOLA + singlet O atom, prior to the secondary oxidation.

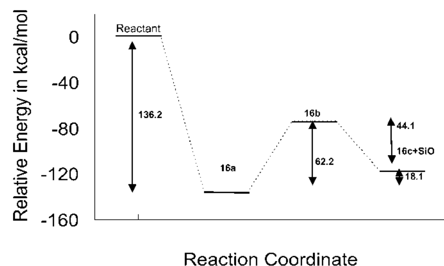

Figure 15. Relative energy diagram along the secondary etching oxygen first mechanism. Energies are obtained with SIMOMM:MRMP2(12,11)/6-311G(d)/HW(d) at SIMOMM:CASSCF(8,8)/HW(d) geometries.

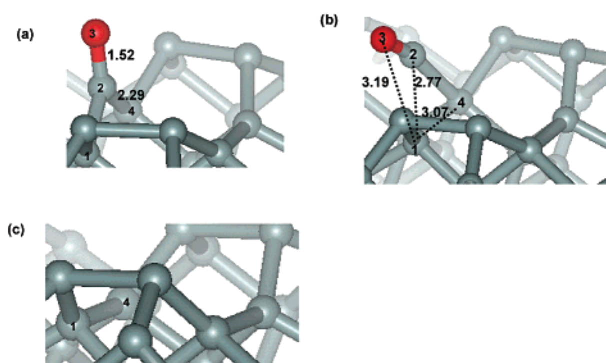

Figure 16. The minima and transition state along the secondary etching oxygen first reaction path, obtained with SIMOMM:CASSCF(8,8)/HW(d): (a) silanone structure; (b) transition state connecting a and c; and (c) surface with the Si dimer etched.

adsorbed O could influence (and facilitate) subsequent SiO desorption and etching. Here, we just consider one possibility where the desorbing SiO is adjacent to a single vacancy. Once one of the Si atoms of the surface dimer is etched, the other Si atom becomes a surface silylene (see atom 4 in Figure 11b). So a "secondary oxidation" may occur at the remaining Si atom. Once the second SiO leaves the surface, the surface will undergo relaxation as shown in Figure 11c. To study this part of the potential energy surface, the (8,8) active space shown in Figure 3 was used to optimize the minima and transition states. Energies were obtained with the (12,11) active space that utilizes all of the orbitals shown in Figure 3.

Two mechanisms for the desorption process, referred to as SESF (Secondary Etching-Silicon First) and SEOF (Secondary Etching-Oxygen First), were found. The relative energies for the SEOF mechanism are summarized in Table 4 and Figure 15. These reactants are the precursor silylene (referred to above as SOLA) and atomic oxygen. (Note that all energies are compared with the singlet state of the reactants, SOLA+O(^{1}D).) The corresponding structures are illustrated in Figure 16. The initial secondary oxidized structure is **16a**, the "silanone" structure, which is apparently stabilized since there is no nearby reactive silyene. This structure is 136.8 kcal/mol more stable than the reactants. The desorption transition state, **16b**, connects **16a** and the etched surface **16c** with a 62.2 kcal/mol activation energy (see Figure 15). In **16b**, the Si_1-Si_2 bond is breaking and the initially "perpendicular" Si_2-Si_4 bond is forming. The product, **16c**, is the relaxed surface plus the SiO molecule. The forward activation energy is an estimate of the overall activation energy of the desorption process of the secondary active oxidation. This activation energy is much smaller than the 89.8 kcal/mol overall barrier for the initial oxidation process (see Figure 9). This indicates, as suggested above, that the SiO desorption process becomes more facile in this stage of active oxidation.

Now consider the SESF mechanism. The energies of intermediates and transition states are summarized in Table 5 and Figure 17. The corresponding structures are illustrated in Figure 18. Transition state **18a** connects the initial oxidation structure **16a** with **18b**, in which the oxygen is inserted into the Si2−Si4 bond. Structure **18b** is analogous to the "back-bond" structure discussed previously. The activation barrier for this first step in the SESF mechanism is 34.6 kcal/mol, much lower than the 62.2 kcal/mol barrier to transition state **16b**. Therefore, the initial oxidation state, **16a**, is more easily converted to **18b**. However, note that the reverse barrier **18b** → **16a** is 34.7 kcal/mol, since the stabilities of **16a** and **18b** are nearly the same. So these two structures may be the two most stable initial states in the secondary etching process. The transition state **18c** connects the intermediates **18b** and **18d**, with a 51.0 kcal/mol barrier. The latter structure, formed by breaking the Si1−Si2 bond and making the Si1−O3 bond, has a tricoordinate oxygen. This intermediate is only 0.7 kcal/mol more stable than transition state **18c**. Transition state **18e** connects intermediate **18d** with the final products, **16c** and SiO, with a barrier of 1.9 kcal/mol. In the transition state **18e**, the O3−Si4 bond is being broken and the Si1−Si4 bond is being formed. The net forward barrier for this SESF mechanism is 52.2 kcal/mol, very close to the lower limit of the experimental range of desorption barriers, 40−50 kcal/mol.[28] It is therefore possible that this lower observed activation energy corresponds to secondary etching.

4. Conclusions

The O adsorption and SiO desorption (key steps in passive and active oxidation, respectively) reactions on Si(100) by atomic oxygen were studied using multireference wave functions in combination with a hybrid QM/MM method. The "on-dimer", "dimer-bridge", and "back-bond" structures are found to be stable intermediates, confirming the results of earlier experimental and theoretical studies of the passive oxidation that concluded there are multiple stable initial oxidation species. All three products have significant diradical character. Since their relative energies are all within a 4 kcal/mol range, all three are likely to be populated following the initial passive oxidation. The surface conversion channel between the on-top and on-dimer structures suggests that surface redistributions among the initial surface products are likely, at least at higher temperatures.

The natural orbital occupation numbers (NOON) at several points on the oxidation potential energy surface indicate that the many parts of this surface have significant multiconfigurational character, necessitating the use of MCSCF wave functions. Although most reactants, intermediates, products, and transition states have significant diradical character, once an O atom bonds to the surface, the singlet potential surface is lower than the triplet PES.

Table 5. Relative Energies of Minima and Transition State along the Secondary Etching Path (SESF) (kcal/mol)

	18a, TS	18b	**18c**, TS	18d	**18e**, TS
CASSCF(12,11)/HW(d)	−100.9	−150.5	−105.9	−107.7	−97.1
MRMP2(12,11)/HW(d)	−100.0	−139.5	−86.8	−87.1	−83.7
MRMP2(12,11)/MIXED	−101.6	−136.3	−85.3	−86.0	−84.1

[a] All calculations are done with the SIMOMM($OSi_{14}H_{20}$; $OSi_{135}H_{92}$) model. [b] All geometries are obtained with SIMOMM:CASSCF(8,7)/HW(d). [c] All energies are QM + MM energies. [d] All energies are relative to the reactants, SOLA + singlet O atom.

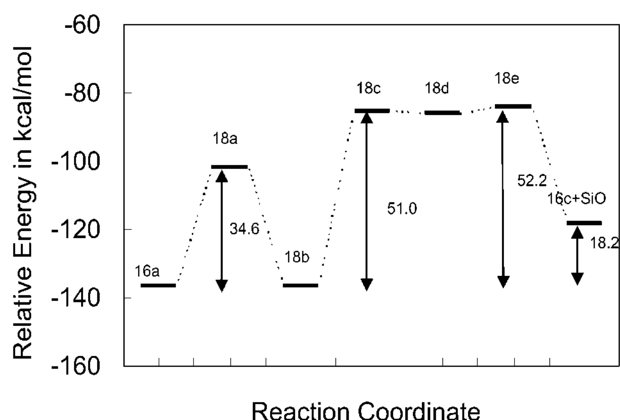

Figure 17. Relative energy diagram along the secondary etching silicon first mechanism. Energies are obtained with SIMOMM:MRMP2(12,11)/6-311G(d)/HW(d) at SIMOMM:CASSCF(8,8)/HW(d) geometries.

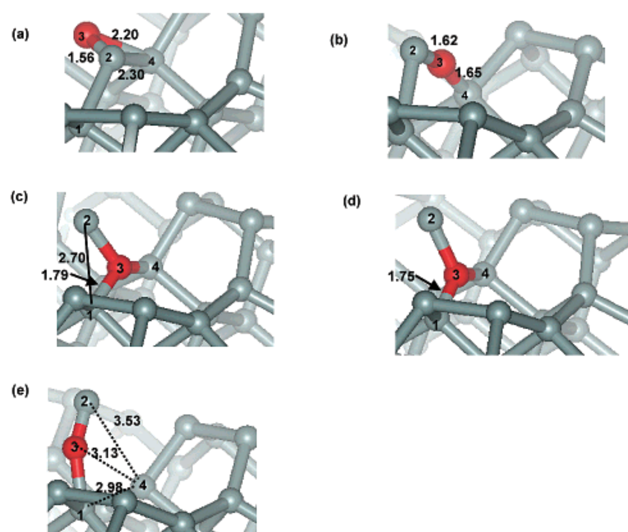

Figure 18. The minima and transition state along the secondary etching silicon first reaction path, obtained with SIMOMM:CASSCF(8,8)/HW(d): (a) transition state connecting **16a** and b; (b) backbone structure; (c) transition state connecting b and d; (d) intermediate with tricoordinated oxygen; and (e) transition state connecting d and **16c**.

Two SiO desorption (etching) mechanisms, the silicon-first (SF) and oxygen-first (OF) leaving mechanisms, have been found. Both mechanisms start from the back-bond configuration. The SF reaction path contains two transition states and two intermediates, with the highest barrier well below the initial reactants. In contrast, the initial transition state on the OF reaction path requires almost of all the energy gained in the initial passive oxidation. The calculated SiO desorption barrier for both channels is 89.8 kcal/mol, in excellent agreement with the upper limit experimental values, 80−90 kcal/mol. This supports the mechanisms proposed here.

The often proposed surface silanone does not appear to exist, at least not when there is a nearby reactive silyene. Our suggested mechanism as shown in Figure 14 is fundamentally different from the commonly held view, which involves the additional assumptions leading to the dual species model (see Section 3.E). A "single" species model (with only strongly bound readily interconverting adsorbed oxygen species) can likely explain experimental observations given the highly cooperative nature of etching and oxide formation processes. This issue will be pursued in future work.

Once Si atoms have been etched from the surface, vacancies or defects are produced. Nearby these defects, modified Si−Si surface bonding results in surface relaxation. This relaxation can activate the nearby surface facilitating subsequent oxidation. An example of this behavior type is the proposed "secondary etching" mechanism that resulted in desorption channels with low activation barriers of 50−60 kcal/mol. These values are significantly smaller than the initial active oxidation barrier but comparable with lower experimental values of 40−50 kcal/mol. Thus, one explanation for the rather wide variation in the observed activation barriers is that different desorption barriers can apply to different stages of the overall active oxidation process.

Acknowledgment. C.H.C. and M.S.G. were supported by a DoD CHSSI grant for software development and by a grant from the Air Force Office of Scientific Research. D.J.L. and J.W.E. were supported by the Division of Chemical Sciences, USDOE-BES. The work was performed at Ames Laboratory, which is operated for the USDOE by Iowa State University under Contract No. W-7405-Eng-82. The calculations reported here were performed on 14 node and 64 node PC-clusters provided by the Ames Laboratory-USDOE and an IBM SP2 obtained via grants from the National Science Foundation and AFOSR.

JA012454H